CHEMISTRY
A EUROPEAN JOURNAL

DOI: 10.1002/chem.200801048

VIP

Polymorphic Coordination Networks Responsive to CO_2, Moisture, and Thermal Stimuli: Porous Cobalt(II) and Zinc(II) Fluoropyrimidinolates

Simona Galli,*[a] Norberto Masciocchi,[a] Giulia Tagliabue,[a] Angelo Sironi,[b] Jorge A. R. Navarro,[c] Juan M. Salas,[c] Laura Mendez-Liñan,[c] Maria Domingo,[c] Manuel Perez-Mendoza,[c] and Elisa Barea*[d]

Abstract: The novel porous $[\{M(F\text{-}pymo)_2\}_n]\cdot 2.5n\,H_2O$ coordination networks (M = Co, Zn; F-pymo = 5-fluoropyrimidin-2-olate), possessing sodalitic topology, have been synthesised and structurally characterised by means of powder diffraction methods. Thermodiffractometry demonstrated their plasticity: when heated up to 363 K, they reversibly transform into three-dimensional dehydrated $[\{M(F\text{-}pymo)_2\}_n]$ species, with significantly different lattice parameters. Further heating induces irreversible polymorphic transformations into layered phases, in which the original MN_4 coordination sphere changes into an MN_3O one. A mixed-metal phase, $[\{Co_xZn_{1-x}(F\text{-}pymo)_2\}_n]\cdot 2.5n\,H_2O$, was also prepared, showing that zinc is preferentially inserted, when starting from a Co/Zn reagent ratio of 1:1. The solid–gas adsorption properties of the anhydrous 3D frameworks have been explored towards N_2, H_2 (77 K) and CH_4, CO_2 (273 K). These results show that these materials permit the diffusion of CO_2 molecules only. Remarkably, the CO_2 adsorption process for the $[\{Co(F\text{-}pymo)_2\}_n]$ network proceeds in two steps: the first step takes place at low pressures (< 600 kPa) and the second one above a threshold pressure of 600 kPa. By contrast, the $[\{Zn(F\text{-}pymo)_2\}_n]$ network only permits CO_2 diffusion by applying pressures above 900 kPa. This type of behaviour is typical of porous networks with gated channels. The high CO_2 selectivity of these systems over the rest of the essayed probe gases is explained in terms of flexibility and polarity of the porous network. Finally, the magnetic studies on the Co^{II} systems reveal that the as synthesised $[\{Co(F\text{-}pymo)_2\}_n]\cdot 2.5n\,H_2O$ material behaves as an antiferromagnet with a T_N of about 29 K. At variance, the $[\{Co(F\text{-}pymo)_2\}_n]$ layered phase shows an unusually weak ferromagnetic ordering below 17 K, arising from a spin-canting phenomenon.

Keywords: adsorption · cobalt · metal–organic frameworks · X-ray diffraction · zinc

Introduction

Open metal–organic frameworks (MOF's) and, particularly, porous coordination polymers (PCP's) have attracted the interest of chemists and material scientists, since the late nineties, with the aim of finding inexpensive, chemically and thermally stable materials for efficient gas storage[1,2] and separation.[3] The pioneering work by Yaghi[4] and Kitagawa[5] was soon followed by a blooming of interesting results, particularly in the field of hydrogen-gas storage for mobile applications, such as fuel cells, electrical power generation for portable PC's, mobile phones and, above all, vehicles.[6] One of the current topics in the design and preparation of PCP's possessing valuable functional properties is the attempt to recreate the topologies of inorganic microporous zeolites, extensively studied and applied in separation, storage, and heterogeneous catalysis.[7] Indeed, PCP's would add to the high thermal stability typical of zeolites, a higher framework flexibility, an easier pore/surface modulation and controllable pore size,[8] as well as additional physicochemi-

[a] Dr. S. Galli, Prof. N. Masciocchi, G. Tagliabue
Dipartimento di Scienze Chimiche e Ambientali
Università dell'Insubria, via Valleggio 11, 22100 Como (Italy)
Fax: (+39) 031-326-230
E-mail: simona.galli@uninsubria.it

[b] Prof. A. Sironi
Dipartimento di Chimica Strutturale e Stereochimica Inorganica
Università di Milano, via Venezian 21, 20133 Milano (Italy)

[c] Prof. J. A. R. Navarro, Prof. J. M. Salas, L. Mendez-Liñan, Prof. M. Domingo, Dr. M. Perez-Mendoza
Departamento de Química Inorgánica
Universidad de Granada, Av. Fuentenueva S/N
18071 Granada (Spain)

[d] Dr. E. Barea
Dipartimento di Chimica Inorganica, Metallorganica e Analitica
Università di Milano, via Venezian 21, 20133 Milano (Italy)
Fax: (+39) 02 50314405
E-mail: ebaream@ugr.es

Supporting information for this article is available on the WWW under http://dx.doi.org/10.1002/chem.200801048; it contains the STA curves for the three α-species.

cal properties, such as magnetism, conductivity and optical features.[9] Some advances in this sense have already been done, involving, for example, a class of metal imidazolates.[10,11]

In this context, we have recently prepared and characterised a number of zeolitic PCP's of $[\{M(pymo)_2\}_n]$ formula, based on the deprotonated hydroxypyrimidine (Hpymo) ligands. Metal variation and ligand substitution have been explored as a way to tune the structural aspects and the functional properties of these materials, leading to the discovery of dense 2D and 3D $[\{M(X\text{-}pymo)_2\}_n]$ polymeric species (M = Co, Zn; X-pymo = 5-X-pyrimidin-2-olate; X = NO_2,[12] Cl, Br, I[13]), or of porous materials, for example, the sodalitic $[\{Cu(H\text{-}pymo)_2\}_n]$[14] and $[\{Pd(X\text{-}pymo)_2\}_n]$ (X = H, F)[15] materials, and the gismondine-like $[\{Cu(F\text{-}pymo)_2\}_n]$[16] one. It is worth noting the solid–gas adsorptive properties of the last system, which gives rise to an unusual ordering of the stored gas molecules related to their ultramicroporous nature.[17]

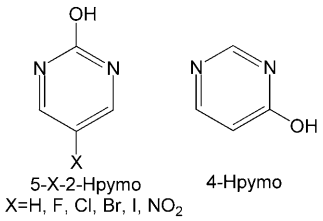

Prompted by these results, in search for new porous species with increased functionality, we began to explore other metal–ligand combinations. In this paper, we present the new $[\{M(F\text{-}pymo)_2\}_n]\cdot 2.5n\,H_2O$ systems (M = Co, Zn), which show a number of solid-to-solid, reversible or irreversible phase changes, also involving polymorphic species. Overall, these phase transformations allowed the isolation of 2D dense phases or 3D porous frameworks, the latter being capable to accommodate H_2O or CO_2 molecules within their nanometer-sized cavities with concomitant induced phase changes.

Thermal analyses (TG, DSC), X-ray powder diffraction (XRPD) structural determinations, thermodiffractometry (TXRPD), electronic spectroscopy, magnetic and gas adsorption measurements have been employed to give a coherent picture of this complex system, aiming at investigating and optimising its functionalities. For the sake of comprehension, the reader is referred to Scheme 1, in which the phases later discussed, together with the labels adopted throughout the paper, are reported.

Results and Discussion

Synthesis: The reaction of $M(NO_3)_2\cdot 6H_2O$ (M = Co, Zn) salts with F-pymo (F-pymo = 5-fluoropyrimidin-2-olate) in aqueous solutions affords microcrystalline materials of formula $[\{M(F\text{-}pymo)_2\}_n]\cdot 2.5n\,H_2O$ (M = Co (α-**Co**) or Zn (α-**Zn**)). The insolubility of these systems in common organic solvents suggests their polymeric nature. In addition, we have demonstrated that the formation of mixed-metal phases is also possible. Indeed, in the presence of a Co/Zn 1:1 ratio, the $[\{Co_{0.21}Zn_{0.79}(F\text{-}pymo)_2\}_n]\cdot 2.5n\,H_2O$ (α-**CoZn**)

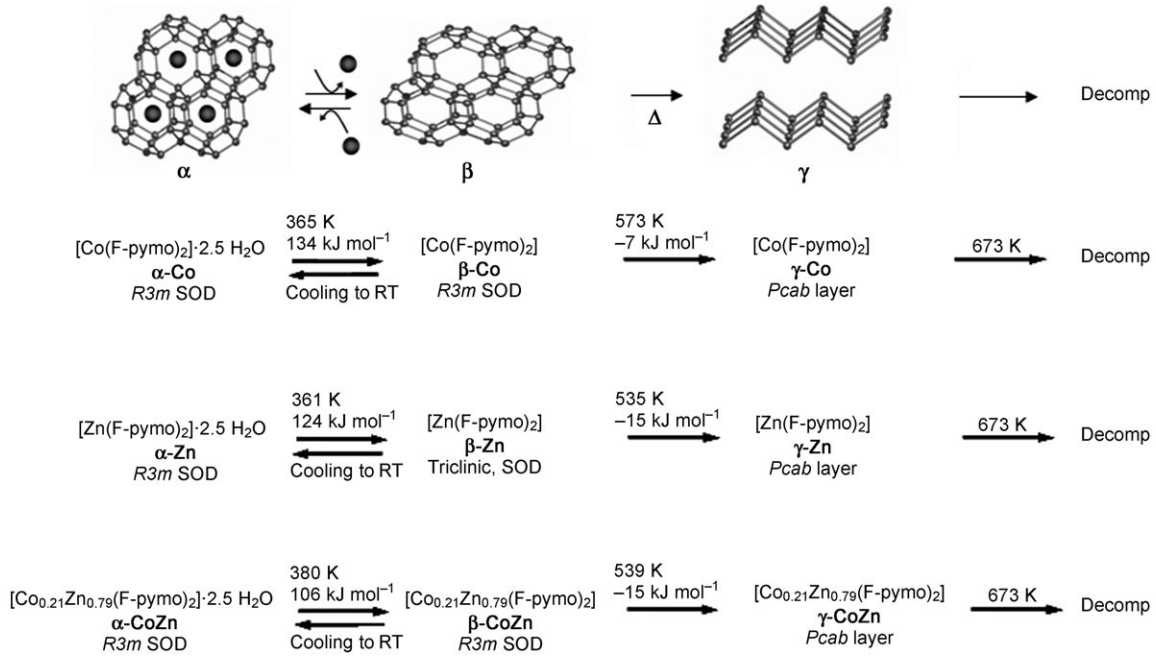

Scheme 1. Summary of the observed structural transformations for the Co, Zn and mixed Co/Zn 5-fluoropyrimidinolates, highlighting the thermal properties and transformation temperatures, determined through a complementary use of thermodiffractometry and simultaneous thermal analysis (sweeping rate 20 K min^{-1}).

species may be isolated, as revealed by an X-ray fluorescence (XRF) quantitative analysis. This occurrence suggests that zinc(II) is preferentially included during the synthesis of the mixed-metal system. To further support this observation, a synthesis was carried out in the presence of a Co/Zn 1:3 ratio, yielding a compound with an almost negligible Co^{II} content, consistent with the formula $[\{Co_{0.02}Zn_{0.98}(F\text{-}pymo)_2\}_n]\cdot 2.5n\,H_2O$ (α-**CoZn′**, XRF evidence). On the other hand, heating of the α-phases under nitrogen afforded, progressively, two novel species (Scheme 1). Indeed, as detailed in the section below, when α-**Co**, α-**Zn** and α-**CoZn** are heated above 360 K, the anhydrous $[\{M(F\text{-}pymo)_2\}_n]$ species (β-**Co**, β-**Zn** and β-**CoZn**, respectively) are obtained. Further heating above 530 K yields the $[\{M(F\text{-}pymo)_2\}_n]$ polymorphs (γ-**Co**, γ-**Zn** and γ-**CoZn**, respectively).

Thermal behaviour of the α-phases: Possibly due to their strict isomorphism (see below), all the α-phases show similar, yet not identical, responses when exposed to progressive heating. To facilitate the comprehension of the following discussion, the thermal behaviour of all the investigated species has been sketched in Scheme 1.

*$[\{Co(F\text{-}pymo)_2\}_n]\cdot 2.5n\,H_2O$ (α-**Co**)*: As regards α-**Co**, a simultaneous thermal analysis (STA) showed that it undergoes a mass loss of about 14% at 365 K, by means of an endothermic process ($\Delta H = 134\ kJ\,mol^{-1}$). The mass loss is compatible with the release of all the clathrated water molecules (theoretical value 13.6%) to form the anhydrous $[\{Co(F\text{-}pymo)_2\}_n]$ (β-**Co**) phase. This phase undergoes a temperature-promoted exothermic transformation ($\Delta H = -7\ kJ\,mol^{-1}$) at 573 K, without any mass loss, yielding a polymorphic form of β-**Co**, namely γ-**Co**, which is stable up to 673 K, when decomposition starts. The TXRPD experiments carried out on α-**Co** further substantiated the STA observations, and concomitantly proved that 1) both the α-**Co**→β-**Co** and β-**Co**→γ-**Co** transformations directly yield the final products and 2) the α-**Co**→β-**Co** phase change is fully reversible, while the β-**Co**→γ-**Co** one is not, allowing γ-**Co** to be recovered at room temperature. Notably, the X-ray powder diffractograms of β-**Co** were of sufficient quality to permit its complete structural characterisation (see below); at variance, the modest crystallinity of the γ-**Co** compound (both at high and at room temperature) only allowed us to assign the lattice metrics and the space group symmetry, thanks to its isomorphism with the Zn^{II} analogue (see the Experimental Section).

An investigation of the thermal behaviour was carried out in the case of β-**Co**, by performing a parametric Le Bail refinement[18] of the unit cell parameters (see the Experimental Section). The increase in temperature promotes a non-negligible increase of the *a* and *c* axes, particularly of the latter, increasing by nearly 2% (Figure 1). Possibly, this may be due to the fact that, within a rhombohedral lattice, the *c* axis constitutes a preferential direction of response to external perturbations. The structural interpretation of this anisotropic lengthening is provided below. Notably, the sodalitic

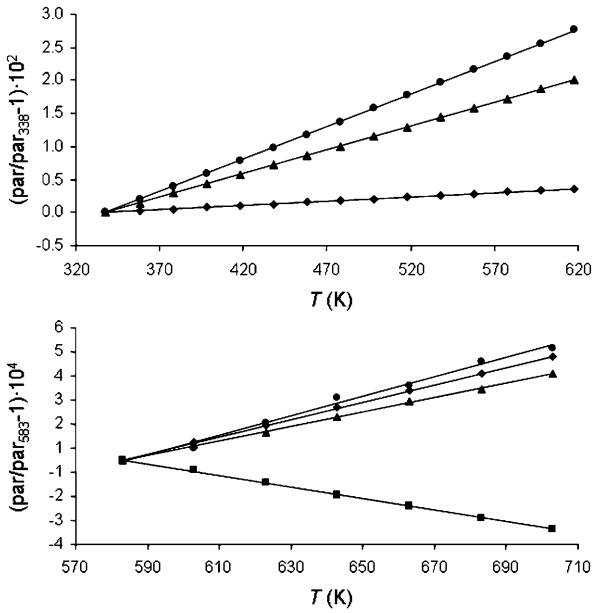

Figure 1. Graphical representation of the relative changes (Δpar/par) for the crystal cells of the β-**Co** species in the 338–618 K range (top) and of the γ-**Zn** one in the 583–703 K range (bottom), as obtained from a Le Bail parametric refinement. *a* (diamonds), *b* (squares), *c* (triangles) and *V* (circles). The absolute temperature values detected during the TXRPD experiments differ from those observed by the STA experiments (see the Experimental Section for the explanation)

metal pyrimidinolates characterised up to now showed a completely different behaviour, upon heating, in terms of flexibility: for the cubic, sodalitic $[\{Pd(F\text{-}pymo)_2\}_n]$ species, the thermal perturbation is isotropic and of much lower entity; for example, a $\partial V/\partial T$ value of $5\times10^{-6}\ K^{-1}$ was computed,[15] to be compared to the ten times higher value of β-**Co** ($5\times10^{-5}\ K^{-1}$).

*$[\{Zn(F\text{-}pymo)_2\}_n]\cdot 2.5n\,H_2O$ (α-**Zn**)*: In the case of α-**Zn**, an STA analysis showed that the compound suffers a mass loss of about 13.5% at 361 K, promoted by an endothermic process ($\Delta H = 124\ kJ\,mol^{-1}$). The mass loss is consistent with the release of all the clathrated water molecules to form the anhydrous $[\{Zn(F\text{-}pymo)_2\}_n]$ species, β-**Zn**. This species undergoes a temperature-promoted exothermic transformation ($\Delta H = -15\ kJ\,mol^{-1}$) at 535 K, without any mass loss. The obtained $[\{Zn(F\text{-}pymo)_2\}_n]$ polymorph (γ-**Zn**) is stable up to 673 K, when decomposition starts. As in the case of the Co^{II} analogue, the TXRPD experiments carried out on α-**Zn** showed that both the α-**Zn**→β-**Zn** and the β-**Zn**→γ-**Zn** transformations directly yield the final product, with no amorphous intermediates. Notably, at variance with γ-**Co**, γ-**Zn** was recovered as a highly (poly)crystalline material at room temperature, thus allowing its structure determination by XRPD methods. Moreover, while the α-**Co**→β-**Co** phase change does not alter the space group, the α-**Zn**→β-**Zn** one clearly implies a symmetry loss, as witnessed by the manifest splitting of the XRPD peaks (Figure 2).

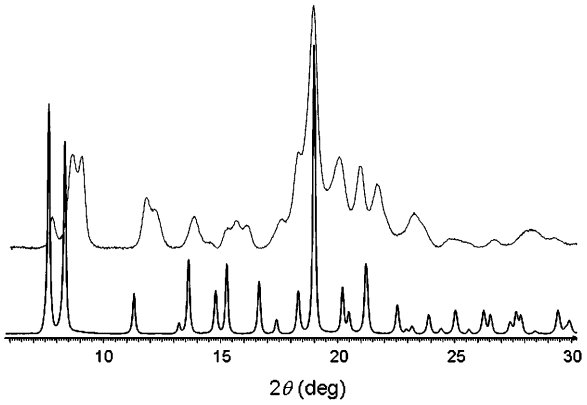

Figure 2. Comparison between the raw diffractograms of α-**Zn** (bottom) and β-**Zn**, showing peaks splitting and broadening for the trigonal to triclinic (α to β) phase conversion.

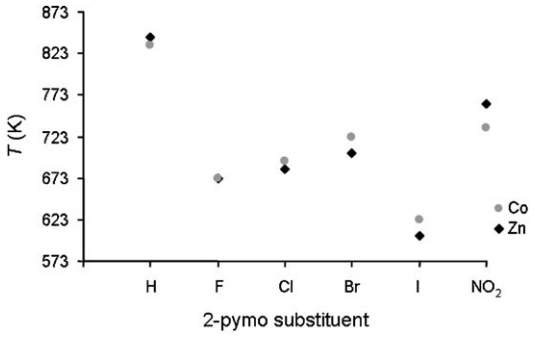

Figure 3. Decomposition temperatures for selected $[\{M(5\text{-}X\text{-}2\text{-}pymo)_2\}_n]$ species, with M = Co, Zn and X = H, F, Cl, Br, I and NO_2. Heating rates in our STA measurements: 20 K min^{-1}.

An analysis of the thermal behaviour was carried out in the case of γ-**Zn**, by performing a parametric Le Bail refinement. On raising the temperature, while the *b* axis shrinks, the *a* and *c* cell axes increase, the cell volume overall slightly expanding, with a volumetric thermal expansion coefficient of only $4\times10^{-6}\,K^{-1}$ (Figure 1).

$[\{Co_{0.21}Zn_{0.79}(F\text{-}pymo)_2\}_n]\cdot 2.5n\,H_2O$ (α-***CoZn***): In spite of the lower percentage of Co^{II} with respect to Zn^{II}, the thermal behaviour of the α-**CoZn** molecular alloy seems to be driven by the former metal. Indeed, as shown by coupling STA and thermodiffractometry, raising the temperature up to 380 K promotes an endothermic process of dehydration ($\Delta H = 106$ kJ mol^{-1}, mass loss = 13.2 %), which yields the β-**CoZn** phase, isomorphous to β-**Co**. Further heating up to 539 K causes an exothermic phase change ($\Delta H = -15$ kJ mol^{-1}) to give the anhydrous γ-**CoZn** species, isomorphous to the γ species of the end members. The compound starts decomposing at about 673 K.

While the trend of the dehydration enthalpies of the α-species cannot be easily explained, the ΔH values of the β-**M**→γ-**M** processes seem to depend on the degree of crystallinity observed by our TXRPD measurements. Thus, α-**Co**, transforming only partially into a highly ordered (crystalline) phase, coherently possesses the least exothermic event at 573 K.

As regards the thermal stability of the $[\{M(5\text{-}X\text{-}2\text{-}pymo)_2\}_n]$ species (M = Co, Zn; X = H, F, Cl, Br, I, NO_2), the highest decomposition temperatures are observed in the presence of the unsubstituted 5-H-2-pymo ligands (Figure 3). Lower thermal stabilities are observed for the halo or nitro substitution, with the I-pymo species showing decomposition temperatures below 673 K, which has been attributed to the intrinsic lability of the I–arene bond.[13]

Crystal structures of the α-phases: The isomorphous α-**Co** and α-**Zn** compounds crystallise in the trigonal *R*3*m* space group. The asymmetric unit is composed of one metal centre, in a general position, one F-pymo ligand in a general position, two F-pymo ligands about a crystallographic mirror plane (*b* Wyckoff position)—giving a total of two ligands per asymmetric unit—and four water molecules, one in a general position and the other three about a crystallographic mirror plane—giving a total of two and a half water molecules per asymmetric unit. Each metal ion possesses a slightly distorted tetrahedral stereochemistry, and is coordinated to four nitrogen atoms belonging to four distinct F-pymo ligands. All the ligands adopt the common N,N′-*exo*-bidentate coordination mode, bridging metal atoms that lie 5.49–5.62 Å apart. Overall, the relative disposition of the bridging ligands promotes the formation of three distinct structural motifs: one rectangular $[\{M(F\text{-}pymo)\}_4]$ motif, which can be ideally described as a metallacalix[4]arene in a 1,3-alternate conformation;[19] two distinct hexagonal $[\{M(F\text{-}pymo)\}_6]$ motifs, one of which is centred about crystallographic 3*m* symmetry sites (Co_6). In both haxagonal motifs, the F-pymo ligands alternately protrude out of, or lie about, the mean plane defined by the metal centres, with three fluorine atoms crowding the hexagonal entrance to the β-cage (Figure 4). The Co_6 ring is linked to consecutive ones by F-pymo bridges running nearly along the *c* direction. On the whole, the mutual interlocking of the three structural motifs results in a polymeric three-dimensional network of the sodalite zeotype (Figure 5). The water molecules occupy the empty space in the cavities (typically referred to as β-cages) and are weakly involved in hydrogen-bond interactions with each other and with the hexocyclic oxygen atoms decorating the cavities' walls. Accordingly, as substantiated by the thermal analyses (see above), they are easily lost upon moderate heating, at about 363 K.

The $[\{Co_{0.21}Zn_{0.79}(F\text{-}pymo)_2\}_n]\cdot 2.5n\,H_2O$ mixed-metal phase α-**CoZn** shares similar structural features with the α-**Co** and α-**Zn** end members. Notably, there is a linear dependence between the unit cell parameters and the Zn^{II} content. Indeed, by applying Vegard's law to the volume of the end members, about 80 % content of Zn^{II} can be estimated in α-**CoZn**, which is in good agreement with the XRF results.

Crystal structure of β-$[\{Co(F\text{-}pymo)_2\}_n]$ (β-Co): Compound β-**Co** crystallises in the trigonal *R*3*m* space group and is iso-

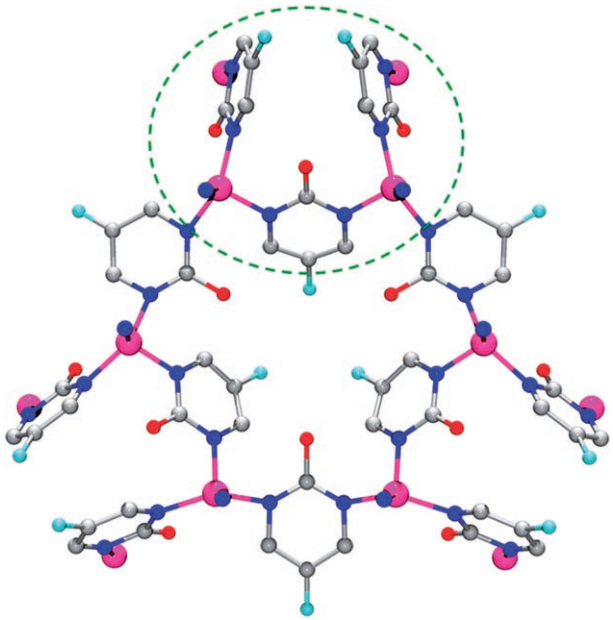

Figure 4. Representation of the hexanuclear [{Co(F-pymo)}$_6$] Co_6 rings in the α-**Co** species, possessing a *3m* symmetry site. Highlighted in a circle: the F-pymo bridges connecting, almost along *c*, consecutive hexagonal motifs. Cobalt: purple; carbon: grey; nitrogen: blue; oxygen: red; fluorine: cyan. The hydrogen atoms have been omitted for the sake of clarity.

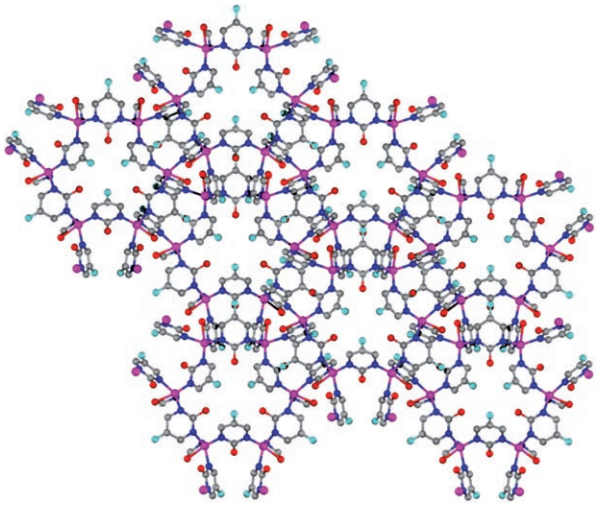

Figure 5. Representation along [001] of the 3D sodalitic network in α-**Co**. At this drawing level, the picture may be considered representative of the sodalitic network found also in the isomorphic α-**Zn** species and in the β-**Co** one. Cobalt: purple; carbon: grey; nitrogen: blue; oxygen: red; fluorine: cyan. The water molecules hosted in the α-**M** systems as well as the hydrogen atoms have been omitted for the sake of clarity.

morphous to α-**Co**. As in the case of α-**Co**, the metal ions, possessing a nearly tetrahedral stereochemistry, are bound to four nitrogen atoms of four distinct F-pymo moieties. All the ligands exhibit a N,N′-*exo*-bidentate coordination mode, bridging metal centres 5.41–5.50 Å apart. Overall, the same structural motifs and three-dimensional network described above for the α-species can be individuated. Thus, thermal annealing promotes water removal with a concomitant cell volume decrease of 13.4%, but leaving the main topological features unaltered. This reasonably contributes to explain the reversibility and rate of the α-**Co**→β-**Co** transformation. Possibly, the observed thermal expansion anisotropy (see above) may be ascribed to the F-pymo ligands bridging the Co_6 hexameric motifs, as if they were slightly reorienting along the *c* axis, the Co_6 hexamers behaving as stiff moieties. Notably, β-**Co** possesses a non-negligible empty volume (13%): the existence of residual empty volume in the anhydrous rhombohedral β-**Co** species may concur to explain the α-**Zn**→β-**Zn** phase change, which implies a more pronounced unit cell volume shrinkage.

Crystal structure of β-[{Zn(F-pymo)$_2$}$_n$] (β-Zn): Even in the absence of a detailed structural model, which could not be derived from XRPD data alone, the similarities among the reduced cells of the four α-**M** and β-**M** species (Table 3), together with the ease of the reversible α→β transformations, allow the derivation of important structural features for β-**Zn**:

1) In spite of the symmetry decrease from the pristine rhombohedral to the triclinic crystal system, the overall network of β-**Zn** is still three-dimensional, with sodalitic topology.
2) The lowering of the crystal system may be attributed to a slight reorientation of the F-pymo ligands.
3) The relative position of the metal centres is basically unchanged.

On the whole, the α-**Zn**→β-**Zn** transformation implies a decrease in molar volume of 24.5%.

Crystal structure of the γ-phases: Compounds γ-**Co**, γ-**Zn** and γ-**CoZn** are isomorphous and crystallise in the orthorhombic space group *Pcab*. Due to its high degree of crystallinity, a complete structure determination was carried out only in the case of γ-**Zn**, on which the following discussion is focused. The asymmetric unit comprises one crystallographically independent metal centre and two crystallographically independent F-pymo ligands, all lying in general positions. Each metal ion possesses a slightly distorted tetrahedral stereochemistry of the ZnN_3O kind, originating from the distinct coordination modes of the two independent F-pymo moieties. Actually, one of the independent F-pymo ligands exploits the *N,N′-exo*-bidentate mode, bridging two metal centres 5.62 Å apart, while the other one adopts the less recurrent *N,O-exo*-bidentate mode, bridging two metal ions separated by 4.83 Å. Metal bridging generates two-dimensional slabs running along *bc* and stacking along *a* (Figure 6). While the *N,N′*-bridging ligands are somehow embedded within the slabs, the *N,O*-bridging ones protrude outside and interdigitate in such a way as to prevent metal bridging along the *a* axis, that is, the creation of a three-dimensional network, and significant inter-slab interactions (shortest inter-slab contact F···N 3.4 Å). It is worth noting

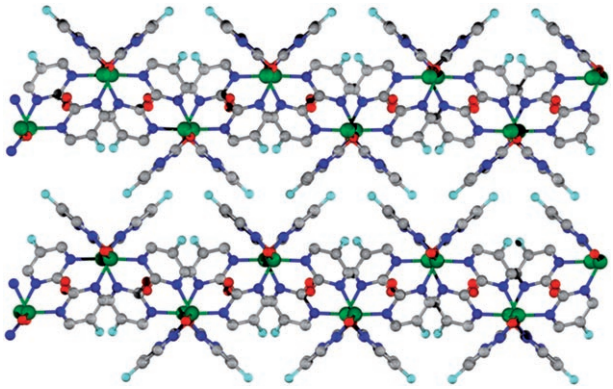

Figure 6. Representation of the two-dimensional slabs running along *bc*, and stacking along *a*, in γ-**Zn**. The *N,O*-bridging ligands, protruding outside and interdigitating in such a way as to prevent metal bridging along the *a* axis, are clearly visible. At this drawing level, the picture may be considered representative of slabs stacking found also in the isomorphic γ-**CoZn** species. Zinc: green; carbon: grey; nitrogen: blue; oxygen: red; fluorine: cyan. The hydrogen atoms have been omitted for the sake of clarity.

that the presence of polymeric slabs adequately substantiates the higher preferred orientation correction ($g = 0.53$ in the March-Dollase formulation[41]) necessary along [1 0 0] when dealing with the XRPD diffractograms of γ-**Zn**. Notably, on assigning the F-pymo ligands as edges and the metal ions as vertices, a wavy structural motif, composed of rectangular meshes of 4.83×5.62 Å^2 dimensions, can be envisaged.

Comparative structural analysis involving the sodalitic species: As already underlined above, the anionic X-pymo ligands, coupled to a variety of transition-metal ions, can afford high-symmetry $[\{M(X\text{-pymo})_2\}_n]$ species belonging to distinct crystal systems: cubic (hydrated and anhydrous $[\{Pd(H\text{-pymo})_2\}_n]$ and $[\{Pd(F\text{-pymo})_2\}_n]$,[15] anhydrous $[\{Cu(H\text{-pymo})_2\}_n]$[14]), trigonal (hydrated $[\{Cu(H\text{-pymo})_2\}_n]$,[14] α-**Co**, α-**Zn**) and tetragonal ($[\{Co(X\text{-pymo})_2\}_n]$ and $[\{Zn(X\text{-pymo})_2\}_n]$ X = H,[20] Cl, Br, I;[13] $[\{Cu(F\text{-pymo})_2\}_n]$[16]). In the following, to derive a comparative structural analysis involving the title compounds, we will focus the discussion on the cubic and trigonal materials. The reader is referred to Table 3, in which the relevant structural parameters of the title compounds are compared with those of $[\{Cu(H\text{-pymo})_2\}_n]$, representative of the previously characterised species.

All the cubic and trigonal species considered here contain 3D frameworks of the sodalite type, based upon X-pymo bridges linking metal ions lying slightly less than 6.0 Å apart, and forming fused four- and six-membered rings, hinged about the M^{II} nodes. The lattice parameters reported in Table 3 clearly speak for a regularity in the overall packing, manifested especially by the limited variability of the *a* and *b* axes. Provided that the space group symmetry and the sodalitic topology are taken into account, even *c* is somewhat constant, with *c*/*a* ratios equal, or slightly lower, than the ideal value of $(3/2)^{1/2}/2 = 0.612$ expected for a trigonal unit cell. The relative distortions from ideal sodalitic frameworks are significant, approaching 23% in the anhydrous β-**Co** phase.

Structurally speaking, the different phases combine distinct stereochemical features dictated, inter alia, by the preferred local coordination geometry of the metal ions: as expected, the MN_4 chromophores are square planar in the cubic phases and in the hydrated $[\{Cu(H\text{-pymo})_2\}_n]$ species,[14] while they are tetrahedral in the cobalt(II) and zinc(II) ones. The most evident consequence of this stereochemical versatility is the relative disposition of the bridging X-pymo ligands to the M···M edges of the sodalitic framework: the 1,3,5-alternate six-membered rings and nearly planar $[\{M(X\text{-pymo})\}_6]$ hexagons of $[\{Cu(H\text{-pymo})_2\}_n]$ significantly change in α-**Co** and α-**Zn** as detailed above.

Another relevant structural parameter, helping the evaluation and comparison of the gas sorption performances of these nanoporous systems, is the empty percent volume,[21] peaking at 43% in the anhydrous $[\{Pd(H\text{-pymo})_2\}_n]$,[15] as low as 13% in β-**Co** and negligible in B-**Zn**.

Comparative structural analysis involving the layered species: While less diffuse than the *N,N′*-exo-bidentate coordination mode, the *N,O-exo*-bidentate mode found in the γ-**c**ompounds has been already exploited by both 4- and 2-pyrimidinolates: indeed, in the $[\{Zn(4\text{-pymo})_2\}_n]$ compound[22] and in the isomorphous $[\{M(5\text{-}NO_2\text{-}2\text{-pymo})_2\}_n]$ (M = Co, Zn) species,[12] the two crystallographically independent ligands concomitantly adopted these two coordination fashions. In the case of $[\{Zn(4\text{-pymo})_2\}_n]$, a three-dimensional topology was generated, while in the $[\{M(5\text{-}NO_2\text{-}2\text{-pymo})_2\}_n]$ materials the same two-dimensional topology as in γ-**Zn** was present, with γ-**Zn** being indeed isomorphous to them. While the *b* and *c* cell parameters of these three isostructural species are highly comparable (9.6084(5), 9.3685(5) Å for γ-**Zn**; 9.6270(3), 9.4320(3) Å for $[\{Zn(5\text{-}NO_2\text{-}2\text{-pymo})_2\}_n]$; 9.6718(7), 9.4462(6) Å for $[\{Co(5\text{-}NO_2\text{-}2\text{-pymo})_2\}_n]$), the *a* axis increases from 21.1279(7) up to 25.3238(8) Å on passing from γ-**Zn** to $[\{Zn(5\text{-}NO_2\text{-}2\text{-pymo})_2\}_n]$ due to the larger dimensions of the -NO_2 (rather than the -F) substituents.

From a topological point of view, two-dimensional layers based on rectangular (or square) $[\{M(pymo)\}_4]$ meshes have been already observed in $[\{M(4\text{-pymo})_2\}_n]$ (M = Co[23] and Ni[22]); in this case, the metal centres were strictly coplanar and, above all, the less common *N,O*-coordination mode was the only type of ligand bridging, even if supported by ancillary M···N long interactions.

Why a three-dimensional sodalitic framework reassembles, upon heating, into a two-dimensional polymorph may be understood by considering that the formation of stable crystalline solids also benefits from the moderate (but significant) increase in energetically favourable dispersion interactions granted by denser polymorphic phases. The pertinent numbers for the sodalitic β-**Co** and β-**Zn** species (1.709 and 1.913 g cm^{-3}, respectively) and their layered γ-counterparts (1.941 and 2.036 g cm^{-3}, respectively) support this interpretation. This behaviour further supports the analogies

between the nature of this kind of system and that of the metastable structurally and functionally related zeolites.[24]

Finally, the [{M(5-X-2-pymo)$_2$}$_n$] species (X = Cl, Br, I), which are isomorphous and of the diamondoid type, possess non-negligible, stabilising O···X interactions that have been used to interpret their whole structure and thermal stability.[13] Evidently, the same interactions cannot be at work in the case of the F-containing derivatives, which adopt the sodalitic or layered structures above described.

Gas adsorption properties: The gas adsorption properties of the evacuated β-**Co** and β-**Zn** materials were evaluated towards N_2 and H_2 at 77 K, and CO_2 and CH_4 at 273 K. The CO_2 and CH_4 adsorption isotherms for the β-**Co** and β-**Zn** phases are shown in Figure 7. The results show that the

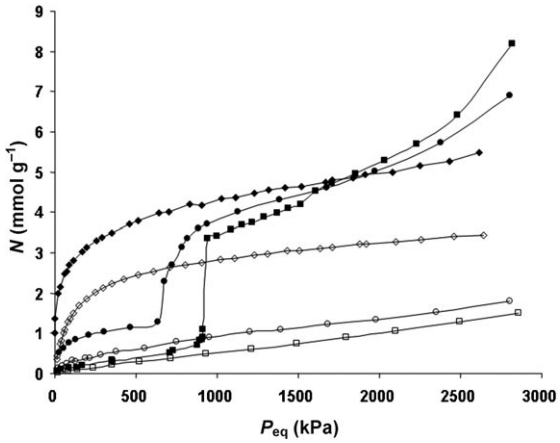

Figure 7. CO_2 and CH_4 adsorption isotherms at 273 K for β-**Co** (circles), β-**Zn** (squares) and [{Cu(H-pymo)$_2$}$_n$] (diamonds). Full and open symbols denote CO_2 and CH_4, respectively.

porous network of these systems does not allow the diffusion of either N_2 or H_2 at 77 K (data not shown). This behaviour agrees with the observed significant shrinkage of the unit cell volume after dehydration (see above) and the probable rigidity of the materials at low temperatures. By contrast, the CO_2 molecules are able to diffuse through the porous network of β-**Co** and β-**Zn** at 273 K. In the case of β-**Zn** there is no CO_2 adsorption up to about 900 kPa. However, above this threshold pressure there is a steep rise in the adsorbed amount of CO_2 reaching a value of 8 mmol g^{-1} at approximately 2800 kPa. At variance in β-**Co**, the adsorption process takes place in two steps. First of all, we see the formation of a reversible type I isotherm with a steep rise in the low-pressure range indicative of moderate permanent porosity, which accounts for a surface area of about 300 m^2 g^{-1} and a micropore volume of 0.11 cm^3 g^{-1} obtained by applying the Dubinin–Radushkevich equation.[25] Afterwards, as in β-**Zn**, there is a sudden rise of the adsorbed amount above a threshold pressure of 600 kPa reaching a value of 7 mmol g^{-1} at 2800 kPa. By contrast, CH_4 molecules are not adsorbed in the whole pressure range studied (up to 2800 kPa) in either β-**Zn** or β-**Co**. The different adsorptive behaviour of these two systems towards N_2 and H_2 at 77 K relative to CO_2 at 273 K should be attributed to both the higher kinetics energy of the CO_2 gas molecules and to the higher thermal energy of the coordination networks themselves at 273 K, which may allow the breathing of the sodalitic hexagonal windows permitting the diffusion of the CO_2 molecules through a narrow porous network.[16] The high CO_2 threshold pressure of the β-**Zn** and β-**Co** phases should be related to their small *V*/*Z* value, which suggests a structural phase-change back to the open α-**Zn** and α-**Co** networks, to accommodate a large amount of CO_2 molecules in their porous networks.[26] The selectivity of CO_2 over CH_4 seems to be related to a probable combination of size-exclusion effects (kinetic diameter 3.3 Å for CO_2 *vs* 3.8 Å for CH_4) and the polar nature of the pore windows. Whilst CO_2 has a significant quadrupole moment (-1.4×10^{-35} C m), CH_4 has no specific moment. In this regard, it seems that the interaction of CH_4 with the porous network is so weak that the applied pressures are not high enough to let the pores of the β-**Zn** and β-**Co** phases "breathe". A related behaviour has been previously described by Férey and coworkers on the MIL-53 material, which shows a remarkable breathing effect upon application of high CO_2 pressures and a high selectivity over CH_4 related to the polar nature of hydrated pores.[27] For comparative reasons, we have also studied the high-pressure performance of the related sodalitic [{Cu(H-pymo)$_2$}$_n$][28] network, which possesses permanent porosity, with approximately 28% empty volume, easily accessible to different probe gases, for example, H_2, N_2, CO (77 K), CO_2 and CH_4 (273 K), at standard low-pressure adsorption conditions. In contrast to the β-**Zn** and β-**Co** phases, the high-pressure adsorption results for [{Cu(H-pymo)$_2$}$_n$] show the formation of type I adsorption isotherms and that considerable amounts of both CO_2 (up to 5.5 mmol g^{-1} at 2600 kPa) and CH_4 (up to 3.5 mmol g^{-1} at 2600 kPa) are adsorbed (Figure 7). The different performance of the [{Cu(H-pymo)$_2$}$_n$] system relative to the β-**Co** and the β-**Zn** phases may be related to a series of features:

1) [{Cu(H-pymo)$_2$}$_n$] possesses segregated polar and apolar pore windows, while all the β-**Co** and the β-**Zn** pore windows are of polar nature.
2) The differences in available pore volume in [{Cu(H-pymo)$_2$}$_n$] (28%) versus β-**Co** (13%) and β-**Zn** (negligible).
3) The isotropic nature of the [{Cu(H-pymo)$_2$}$_n$] system (cubic) versus the anisotropic one of β-**Co** (trigonal) and β-**Zn** (triclinic) (Table 3).

These features apparently result in highly deformed (dense) β-**Co** and β-**Zn** phases and polar channels unsuitable for CH_4 diffusion.

Electronic spectroscopy and magnetic behaviour of α-Co and γ-Co: The electronic absorption spectra of the Co^{II} species α-**Co** and γ-**Co** (Figure 8) and their deep purple colour

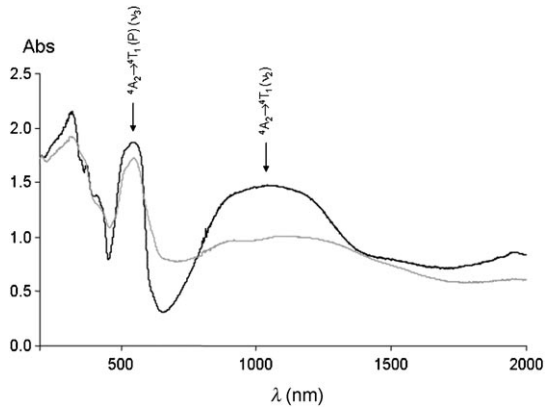

Figure 8. Electronic absorption spectra of α-**Co** (black) and γ-**Co** (grey). The absorption maxima corresponding to the $^4A_2 \rightarrow {}^4T_1$ (ν_2) and $^4A_2 \rightarrow {}^4T_1(P)$ (ν_3) electronic transitions have been indicated in both cases.

are consistent with a tetrahedral environment about cobalt when surrounded by azaaromatic ligands.[12,23,20,29] In the spectra of both species, the absorption bands corresponding to the $^4A_2 \rightarrow {}^4T_1$ (ν_2) (α-**Co**: 9595 cm^{-1}; γ-**Co**: 8890, 10930 cm^{-1}) and $^4A_2 \rightarrow {}^4T_1(P)$ (ν_3) (α-**Co**: 18350, 19455 cm^{-1}; γ-**Co**: 18180, 19050 cm^{-1}) electronic transitions are clearly observed. However, the $^4A_2 \rightarrow {}^4T_2$ (ν_1) one, occurring in the NIR region, is not detectable. It is worth noting that the ν_2 and ν_3 transitions appear as multiple bands, as it is usually found for tetrahedral Co^{II} stereochemistries, which allow an unequivocal distinction from octahedral geometries.[30] In the case of tetrahedral complexes, the position of the maximum of the first electronic transition, ν_1, coincides with the value of Δ_t. Since ν_1 is undetectable in the present case, its value has been calculated from those of ν_2 and ν_3 by applying Dou's method.[31] As ν_2 and ν_3 are multiple bands, an intermediate value of their maxima positions has been taken. The obtained Δ_t values of 5650 cm^{-1} and 5890 cm^{-1} for the α-**Co** and γ-**Co** species, respectively, are in agreement with other Co^{II} species previously described by us, containing tetrahedral metal centres and pyrimidinolate ligands.[22,23,29a] Thus, it can be reasonably concluded that both the position of the exocyclic oxygen atom and the presence of different substituents in the pyrimidine ring only marginally affect the electronic properties of these systems.

The thermal dependence of the magnetic susceptibility for the α-**Co** and γ-**Co** materials is shown in Figure 9. Both of them possess similar magnetic behaviour in the high-temperature region. By contrast, in the low-temperature region, substantially different magnetic behaviours are encountered. Regarding the thermal dependence of the dc magnetic susceptibility (χ_M) for the α-**Co** phase, there is a maximum at about 29 K and a smooth decrease of the $\chi_M T$ values from 1.87 $cm^3 mol^{-1} K$ at 250 K to 0.037 $cm^3 mol^{-1} K$ at 2 K. This behaviour is typical of a system in which a significant antiferromagnetic exchange is at work. The susceptibility data have been satisfactorily fit to the Curie–Weiss equation $\chi_M = C/(T-\theta)$, $[C = Ng^2\mu^2 S(S+1)/3k]$ with $C = 2.28(1)$ $cm^3 K mol^{-1}$, $\theta = -53.1(8)$ K. These values are in the same range as those

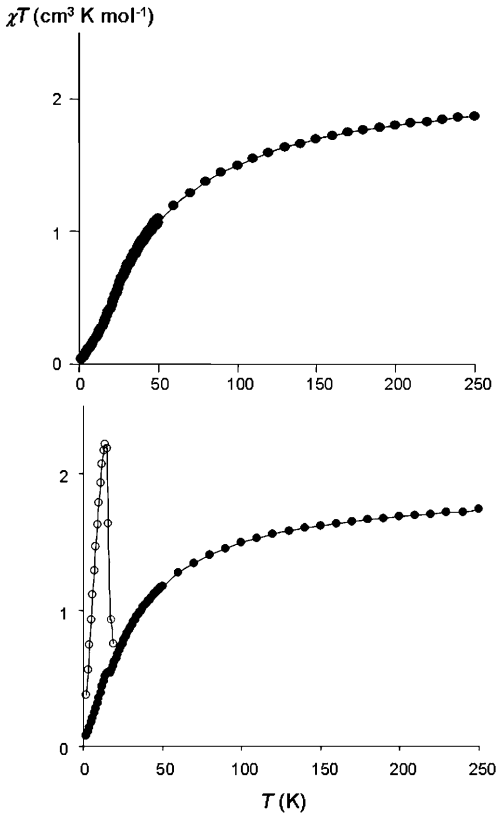

Figure 9. Thermal behaviour of the $\chi_M T$ product for the α-**Co** (top) and γ-**Co** (bottom) phases. Full and open symbols denote measurements applying external magnetic fields of 5000 and 100 Oe, respectively.

found for the 3D diamondoid $[\{Co(X\text{-pymo})_2\}_n]$ (X = Cl, Br, I) series, which further agrees with the efficiency of the *N,N′*-pymo bridges to transmit a magnetic interaction.[13] Likewise, the high-temperature behaviour of the dc magnetic susceptibility for γ-**Co** is typical of an antiferromagnetic material with a maximum at about 18 K and the $\chi_M T$ values showing a smooth decrease from 1.74 $cm^3 mol^{-1} K$ at 250 K to 0.56 $cm^3 mol^{-1} K$ at 18 K. Its susceptibility data have been fit to the Curie–Weiss equation, $\chi_M = C/(T-\theta)$, with $C = 1.94(1)$ $cm^3 K mol^{-1}$ and $\theta = -32.4(4)$ K. For both compounds, the behaviour described is due to the antiferromagnetic coupling of the cobalt(II) centres transmitted through the *N,N′*- and *N,O*-F-pymo bridges. Alternatively, the magnetic behaviour of γ-**Co** can be reasonably interpreted through Equation (1), which is adequate to describe the high-temperature dependence of $\chi_M T$ on a 2D Heisenberg quadratic network of spins.

$$\chi T = \frac{Ng^2\mu_B^2 T}{J\left(3\theta + \sum_{n=1}^{\infty} \frac{C_n}{\theta^{n-1}}\right)} \quad (1)$$

In Equation (1) the spin Hamiltonian is defined as $H = \Sigma J \cdot S_i S_j$,[32] $\theta = kT/JS(S+1)$, g is the Landè factor, μ_B is the Bohr magneton and N is the number of spins in the lattice; the C_n coefficients have been taken from reference [32b].

Fitting the data to Equation (1), g and J exchange values of 2.031(2) and $-3.76(4)$ cm^{-1} were obtained. The J exchange value found for γ-**Co** is comparable to that obtained for the related layered $[\{Co(5\text{-}NO_2\text{-}pymo)_2\}_n]$ system ($-4.82(2)$ cm^{-1}), with the 5-nitropyrimidine-2-olate ligand exhibiting both the *N,N′*- and the *N,O-exo*-bidentate coordination mode.[12]

It should be noted that, below the Néel temperature T_N (ca. 17 K), the magnetic susceptibility of the γ-**Co** phase shows a change in its trend, with the χ_M and $\chi_M T$ values sharply increasing and becoming field dependant. Thus, at an external field of 100 Oe, the $\chi_M T$ values reach a maximum value of 2.22 $cm^3 K mol^{-1}$ around 14 K. The sharp increment of the χ_M and $\chi_M T$ values in the low-temperature region and at low field strengths suggests a weak ferromagnetic ordering arising from a spin-canting phenomenon. This is unequivocally a trace of a partial ordering of the spins at low temperature. However, this canting phenomenon should be symmetrically forbidden, as the $[\{Co(F\text{-}pymo)_2\}_n]$ layers containing the magnetically active centres are centrosymmetric (see the description above). To match (room-temperature) crystallographic and (low-temperature) magnetic evidence, one of the following events (or both) might occur: 1) the structure at low temperature may be slightly distorted, through a structural (perhaps displacive) phase transition (which we cannot measure) or 2) the magnetic lattice does not coincide with the crystallographic one. Indeed, magnetic domains may form because of the symmetry.[33] The ac susceptibility measurements do not show any signal, which agrees with a hidden spin-canted behaviour.

Conclusion

In this work, we proved the suitability of the self-assembly process between transition-metal ions and symmetric pyrimidinolates to build extended open coordination networks. The modification of these systems' properties by external stimuli (temperature, guest molecules) is also worth noting. The structural changes taking place upon application of high-pressure gases, moisture or thermal treatment, with formation of either sorbatomorphic or polymorphic materials, are indicative of unusually flexible coordination networks. The remarkable CO_2 selectivity over CH_4 under high-pressure conditions of this type of systems may open a way for practical separation purposes. It is also worth noting that, although the end members $[\{M(F\text{-}pymo)_2\}_n]\cdot 2.5nH_2O$ (α-**M**) and $[\{M(F\text{-}pymo)_2\}_n]$ (γ-**M**) are isomorphous, the intermediate $[\{Co(F\text{-}pymo)_2\}_n]$ (β-**Co**) and $[\{Zn(F\text{-}pymo)_2\}_n]$ (β-**Zn**) phases are not. Finally, we should highlight that, in the absence of suitable single crystals, all the valuable structural information presented on the title PCP's have been retrieved by applying ab initio XRPD structure solution methods, sagaciously coupled to thermal XRPD investigations.[34]

Experimental Section

Starting materials (5-fluoro-2-hydroxypyrimidine and metal nitrate salts) were purchased from Sigma-Aldrich and used as received.

Synthesis of the $[\{M(F\text{-}pymo)_2\}_n]\cdot 2.5n\,H_2O$ (α-Co and α-Zn) phases: $M(NO_3)_2\cdot 6H_2O$ (2 mmol) was dissolved in distilled water (10 mL) and 5-fluoro-2-hydroxypyrimidine (4 mmol dissolved in 20 mL of water) was added under stirring. The clear solutions were kept at room temperature for about 20 min and then the pH was raised to 5.0 by addition of 1 M NaOH. The purple (α-**Co**) and white (α-**Zn**) precipitates were filtered off and washed with water, ethanol and diethyl ether. Yield: 60–70 %. elemental analysis calcd (%) for $C_8H_9CoF_2N_4O_{4.5}$: C 29.11, N 16.97, H 2.56; found: C 28.83, N 16.96, H 2.56; elemental analysis calcd (%) for $C_8H_9F_2N_4O_{4.5}Zn$: C 29.24, N 17.05, H 2.76; found: C 28.87, N 16.82, H 2.67.

Synthesis of $[\{Co_{0.21}Zn_{0.79}(F\text{-}pymo)_2\}_n]\cdot 2.5n\,H_2O$ (α-CoZn): $Co(NO_3)_2\cdot 6H_2O$ (1 mmol) and $Zn(NO_3)_2\cdot 6H_2O$ (1 mmol) were dissolved together in distilled water (10 mL) and 5-fluoro-2-hydroxypyrimidine (4 mmol dissolved in 20 mL of water) was added under stirring. The clear solution was kept at room temperature for about 20 min and then the pH was raised to 5.0 by addition of 1 M NaOH. The pale purple (α-**CoZn**) precipitate was filtered off and washed with water, ethanol and diethyl ether. Yield: 60–70 %; elemental analysis calcd (%) for $C_8H_9Co_{0.2}F_2N_4O_{4.5}Zn_{0.8}$: C 29.13, N 16.17, H 2.65; found C 28.66, N 16.71, H 2.70.

Synthesis of $[\{M(F\text{-}pymo)_2\}_n]$ (γ-M) phases: α-**Co** or α-**Zn** (50 mg) were heated up to 600 K, under nitrogen at a heating rate of 20 $K min^{-1}$ affording purple and white microcrystalline phases of $[\{Co(F\text{-}pymo)_2\}_n]$ (γ-**Co**) and $[\{Zn(F\text{-}pymo)_2\}_n]$ (γ-**Zn**), respectively. Yield 100 %; elemental analysis calcd (%) for $C_8H_4F_2CoN_4O_2$: C 33.71, N 19.65, H 1.41; found: C 33.56, N 1.37, H 19.42; elemental analysis calcd (%) for $C_8H_4F_2N_4O_2Zn$: C 32.96, N 19.22, H 1.38; found: C 32.35, N 18.69, H 1.06.

Synthesis of $[\{Co_{0.21}Zn_{0.79}(F\text{-}pymo)_2\}_n]$ (γ-CoZn): α-**CoZn** (50 mg) was heated up to 540 K under nitrogen at a heating rate of 20 $K min^{-1}$ affording a pale purple phase of $[\{Co_{0.21}Zn_{0.79}(F\text{-}pymo)_2\}_n]$ formula (γ-**CoZn**). Yield 100 %; elemental analysis calcd (%) for $C_8H_4Co_{0.2}F_2N_4O_2Zn_{0.8}$: C 33.11, N 19.30, H 1.39; found: C 32.74, N 19.91, H, 1.47.

X-ray powder diffraction analysis: Polycrystalline samples of the investigated phases were manually ground in an agate mortar and then deposited in the hollow of an aluminium holder equipped with a quartz monocrystal zero background plate. All the diffraction data ($Cu_{K\alpha}$, 1.5418 Å) were collected on a θ:θ Bruker Axs D8 Advance vertical scan diffractometer; the generator was operated at 40 kV and 40 mA. For all the species but the α-**Co** alloy, the diffractometer was equipped with a Ni filter and a linear position sensitive detector (PSD), with the following optics: primary and secondary Soller slits, 2.3 and 2.5°, respectively; divergence slit, 0.3°; receiving slit, 8 mm. The nominal resolution for this setup was 0.08° 2θ (FWHM of the α_1 component) for the LaB_6 peak at about 21.3° (2θ). In the case of α-**Co**, the diffractometer was equipped with a secondary beam-curved graphite monochromator, a Na(Tl)I scintillation detector and pulse height amplifier discrimination, with primary and secondary Soller slits, 2.3°; divergence slit, 0.5°, antiscatter slit, 0.5°, receiving slit 0.2 mm. The nominal resolution for this setup was 0.07° 2θ (FWHM of the α_1 component) as measured from the Si(111) peak at 28.44° (2θ). When indexing seemed viable, overnight scans were performed in the 5–105° 2θ range, with $\Delta 2\theta = 0.02°$. Due to their metastable nature, data collections of the β-phases were carried out at 403 K, taking advantage of the experimental setting described in the next paragraph.

Indexing was performed in all cases with the aid of the single-value decomposition approach,[35] as implemented in the TOPAS-R suite of programs[36] (see Table 1 for details). For the trigonal compounds, in the absence of extinction conditions other that those due to lattice centring, the space groups $R3$, $R\bar{3}$, $R32$, $R3m$ and $R\bar{3}m$ were equally good candidates. Eventually, $R3m$ was chosen after a large number of tests, including fruitless structure solution attempts in some of the discarded space groups. In the case of γ-**Zn** and γ-**CoZn**, the orthorhombic space group *Pcab* was assigned on the basis of the systematic extinction conditions and of the

Table 1. Synoptic collection of the unit cell parameters for all of the indexed phases, as resulting from Le Bail or Rietveld refinements, the former carried out when the complete structural model was not available.

	a [Å]	b [Å]	c [Å]	α [°]	β [°]	γ [°]	V [Å^3]	V/Z [Å^3]	R_p	R_{wp}
α-**Co**	23.059	23.059	12.505	90	90	120	5758.4	319.5	0.026 [b]	0.044
α-**CoZn**[a]	23.230	23.230	12.572	90	90	120	5874.1	326.3	0.080	0.107
α-**Zn**	23.279	23.279	12.583	90	90	120	5905.8	328.1	0.059	0.080
β-**Co**	23.641	23.641	10.299	90	90	120	4985.2	276.9	0.020	0.030
β-**CoZn**[a]	23.934	23.934	10.165	90	90	120	5042.9	280.2	0.021	0.027
β-**Zn**[a]	11.293	12.491	12.699	106.07	107.64	105.24	1518.3	253.0	0.010	0.014
γ-**Co**[a]	22.017	9.450	9.372	90	90	90	1950.2	243.8	0.005	0.008
γ-**CoZn**[a]	21.214	9.566	9.366	90	90	90	1900.7	237.6	0.007	0.012
γ-**Zn**	21.128	9.608	9.368	90	90	90	1901.8	237.7	0.118	0.163

[a] Le Bail refinement results. [b] The significantly low agreement factors are mostly due to the high background levels, due to unavoidable Co K fluorescence effects.

comparison of their diffractograms with those of the [{M(5-NO_2-2-pymo)$_2$}$_n$] (M = Co, Zn) species,[12] with which γ-**Zn** (and γ-**CoZn**) eventually proved to be isomorphous. All the chosen (trigonal or orthorhombic) space groups were later confirmed by successful solutions and refinements. In the XRPD pattern of the γ-**Co** species, only a few peaks were visible, lying at 2θ angles similar to those of the layered γ-**Zn** material, possibly suggesting their isomorphous character. After assigning the Miller indices to the γ-**Co** reflections on the basis of those of the γ-**Zn** phase, a least-squares refinement of the resulting lattice parameters was performed using UNITCELL,[37] followed by a Le Bail refinement (Table 1), highlighting the purported isomorphism between γ-**Co** and γ-**Zn**. In contrast, the XRPD pattern of β-**Zn**, very distinct from that of the β-**Co** counterpart, showed many rather broad peaks, consistent with a structure of lower metric symmetry. The observed symmetry was interpreted as a change of the trigonal R crystal system down to triclinic, with a unit cell comparable with the rhombohedral description of the pristine trigonal one, which was indeed the case (a = 11.29, b = 12.49, c = 12.70 Å, α = 106.1, β = 107.6, γ = 105.2°, V = 1518 Å^3 versus a = 14.09 Å, α = 111.5°, V = 1973 Å^3, respectively). Table 1 gives the unit cells for all of the indexed phases, resulting from Le Bail or Rietveld refinements; the former were carried out when the complete structural model was not accessible.

Structure solutions for the archetypical α-**Co** and γ-**Zn** phases were performed by using the simulated annealing technique[38] implemented in TOPAS-R. The F-pymo ligands were treated as rigid bodies, adopting the geometrical parameters derived from ab initio quantomechanical computations.[39] The final refinements were performed by the Rietveld method using TOPAS-R. In the case of α-**Zn** and β-**Co** a Rietveld refinement was directly performed assuming, as a starting point, the α-**Co** model (with or without the water molecules, respectively). Peak shapes were described by the fundamental parameters approach.[40] The experimental background was fit by a polynomial description. Systematic errors were modelled with sample-displacement angular-shift corrections and, in the case of γ-**Zn** only, with a correction of the preferred orientation in the March–Dollase formulation[41] along the [100] pole. Metal atoms were given a refinable, isotropic displacement parameter (B_M), while lighter atoms were assigned a common $B = B_M + 2.0$ Å^2 value. Scattering factors, corrected for real and imaginary anomalous dispersion terms, were taken from the internal library of TOPAS. Final R_p, R_{wp}, R_{Bragg} and details on data collections and analyses can be found in Table 2.

CCDC-689641 (α-**Co**) CCDC-689642 (β-**Co**), CCDC-689643 (α-**Zn**) and CCDC-689644 (γ-**Zn**) contain the supplementary crystallographic data for this paper. These data can be obtained free of charge from The Cambridge Crystallographic Data Centre via www.ccdc.cam.ac.uk/data_request/cif.

Thermodiffractometric measurements: A series of experiments was performed in order to assess the thermal behaviour of the α-phases, by employing a custom-made sample heater (supplied by Officina Elettrotecnica di Tenno, Italy), mounted on the Bruker AXS Advance D8 diffractometer. The compounds were manually ground in an agate mortar, then deposited in the hollow of an aluminium sample holder. Typically, the thermodiffractometric experiment was planned on the basis of the STA results: a sequence of scans, in the 6–21° 2θ range, was performed heating in situ from room temperature up to the temperature at which loss of crystallinity was complete. All the β-phases are unstable at room temperature, so that their complete diffractograms were acquired heating in situ at 403 K, using a silicon monocrystal zero background plate.

To further substantiate the thermal behaviour, the β-**Co** and γ-**Zn** species were chosen as case studies treating, with a Le Bail parametric refinement,[18] their diffraction data acquired in the 338–618 K and 583–703 K ranges, respectively. Note that the absolute temperature values detected during the TXRPD experiments differ from those observed by the STA measurements: A thermal gradient exists between the temperature measured by the theromo couple of the TXRPD chamber and the actual temperature of the sample, the temperature values measured by the STA apparatus thus being more reliable. On applying the parametric refinement,

Table 2. Crystallographic data and details for the X-ray data collection and analyses for compounds α-**Co**, α-**Zn**, β-**Co** and γ-**Zn**.

	α-**Co**	α-**Zn**	β-**Co**	γ-**Zn**
formula	$C_8H_9CoF_2N_4O_{4.5}$	$C_8H_9F_2N_4O_{4.5}Zn$	$C_8H_4CoF_2N_4O_2$	$C_8H_4F_2N_4O_2Zn$
M_r [g mol^{-1}]	330.12	336.57	285.08	291.53
T [K]	298(2)	298(2)	403(2)	298(2)
system	trigonal	trigonal	trigonal	orthorhombic
space group	*R*3*m*	*R*3*m*	*R*3*m*	*Pcab*
Z	18	18	18	8
a [Å]	23.0595(7)	23.2795(5)	23.6414(6)	21.1279(7)
b [Å]	23.0595(7)	23.2795(5)	23.6414(6)	9.6084(5)
c [Å]	12.5048(5)	12.5834(4)	10.2993(5)	9.3685(5)
V [Å^3]	5758.4(4)	5905.8(3)	4985.2(4)	1901.8(1)
ρ_{calcd} [g cm^{-3}]	1.687	1.678	1.709	2.036
F(000)	2988	3042	2538	1152
μ($Cu_{K\alpha}$) [cm^{-1}]	110.18	30.78	124.51	39.26
2θ range [°]	5–105	5–105	5–105	5–105
N_{data}	5001	5001	5001	5001
N_{obs}	816	705	838	1093
R_p/R_{wp}	0.026/0.044	0.059/0.080	0.020/0.030	0.118/0.163
R_{Bragg}	0.029	0.035	0.030	0.040
V/Z [Å^3]	319.5	328.1	276.9	237.7

Table 3. Space group (SG), unit cell parameters, relative distortion from ideal sodalitic frameworks [$\Delta = 1-(c/a)/(c/a)_{ideal}$, with $(c/a)_{ideal} = 0.612$] for selected, cubic or trigonal, [{M(X-pymo)$_2$}$_n$] species. For the sake of comparison, the primitive unit cell of β-**Zn** and of the anhydrous cubic [{Cu(H-pymo)$_2$}$_n$] phase have been transformed into the corresponding *R*-centred ones.

	SG	a [Å]	b [Å]	c [Å]	α [°]	β [°]	γ [°]	V [Å^3]	Z	V/Z [Å^3]	c/a	Δ
α-**Co**	*R*3*m*	23.06	23.06	12.50	90	90	120	5758	18	319	0.542	0.114
α-**Zn**	*R*3*m*	23.28	23.28	12.58	90	90	120	5906	18	328	0.540	0.118
β-**Co**	*R*3*m*	23.64	23.64	10.30	90	90	120	4985	18	277	0.436	0.228
β-**Zn**	*R*1	18.90	20.13	14.00	89.8	96.0	120.6	4554	18	253	n.a.	n.a.
[{Cu(H-pymo)$_2$}$_n$][a]	$R\bar{3}m$	21.31	21.31	26.10	90	90	120	10266	36	285	1.224[b]	0

[a] See reference [14] for the relationship between the anhydrous cubic and the hydrated rhombohedral phases. [b] In this case, the ideal value of 2× 0.612 should be considered for comparison purposes.

a temperature dependence of the unit cell parameters and of the sample height displacement error was assumed of the kind $par(T) = par_0 \cdot (1 + par_1 \Delta T)$, in which ΔT is the difference between the actual temperature T considered and the lower value of the temperature range in which the parametric refinement is carried out.

Thermogravimetric and calorimetric analysis: Thermogravimetric and differential calorimetric analyses were performed simultaneously, under dinitrogen, on a Netzsch STA 409 PC Luxx instrument (University of Insubria), at a heating rate of 20 K min^{-1}.

X-ray fluorescence analyses: XRF quantitative analyses of the Co/Zn composition in the α-**CoZn** and α-**CoZn′** species were performed with a Panalytical Minipal 2 instrument, equipped with a Cr source, on solutions of the samples in aqueous nitric solution and on an equimolar solution of Co/Zn in aqueous nitric solution (ca. 10^{-2} M) used as the standard. To assess the relative Co/Zn ratio in our samples, we determined the relative intensities of the well-separated K-lines fluorescence peaks of their solutions, normalised to the values observed for the standard equimolar solution of Co/Zn. By this method, requiring only a careful weighing of the original salts for the preparation of the reference solution, and, if necessary, long(er) counting times (up to 30 min for the less concentrated solutions), accuracy levels down to about 1% can be achieved.

Magnetism: Magnetic measurements were performed on polycrystalline samples on a SQUID Quantum Design MPMS XL-5 (University of Granada) in the temperature range 2–300 K applying external fields of 5000 and 100 Oe. The ac measurements were performed in the temperature range 2–30 K applying an external field of 1 Oe and a frequency of 100 Hz.

Gas adsorption measurements: Adsorption isotherms were measured on a Micromeritics 2010 M (Instituto Nacional del Carbón, CSIC, Oviedo) and on a Micromeritics Tristar 3000 (University of Granada) volumetric instrument. High-pressure adsorption isotherms were measured in a home-made volumetric adsorption instrument (University of Granada) equipped with two Baratron absolute pressure transducers (MKS type 627B). Their pressure ranges are from 0 to 133.33 kPa and from 0 to 3333.25 kPa, respectively, and the reading accuracy was 0.05% of the usable measurement range. Prior to measurement, powder samples were heated at 303 K for 12 h and outgassed to 10^{-6} Torr using a Micromeritics Flowprep.

Acknowledgement

The authors thank the support of the Spanish Ministry of Education and Science and Italian Ministero dell'Istruzione, Universtità e Ricerca (MIUR) for the projects: CTQ2005-00329/BQU, CTQ2008-0037/PPQ, PRIN 2006: "Materiali ibridi metallo-organici multifunzionali con leganti poliazotati", and Azione Integrata Italia-Spagna HI2006-0116. We also acknowledge the financial support by the Fondazione CARIPLO. E.B. thanks the Spanish Ministry of Education and Science for a postdoctoral grant (MEC-EX2004-0612). G.T. thanks MIUR for a doctoral grant (Progetto Giovani 2006). We also thank Dr. J. B. Parra and Dr. C. O. Ania, INCAR, CSIC for H_2 adsorption isotherms.

[1] a) M. Dincă, W. S. Han, Y. Liu, A. Dailly, C. M. Brown, J. R. Long, *Angew. Chem.* **2007**, *119*, 1441–1444; *Angew. Chem. Int. Ed.* **2007**, *46*, 1419–1422; b) A. R. Millward, O. M. Yaghi, *J. Am. Chem. Soc.* **2005**, *127*, 17998–17999; c) R. Matsuda, R. Kitaura, S. Kitagawa, Y. Kubota, R. V. Belosludov, T. C. Kobayashi, H. Sakamoto, T. Chiba, M. Takata, Y. Kawazoe, Y. Mita, *Nature* **2005**, *436*, 238–241; d) M. Sabo, A. Henschel, H. Fröde, E. Klemm, S. Kaskel, *J. Mater. Chem.* **2007**, *17*, 3827–3832.

[2] a) G. Ferey, *Chem. Soc. Rev.* **2008**, *37*, 191–214; b) R. E. Morris, P. S. Wheatley, *Angew. Chem.* **2008**, *120*, 5044–5059; *Angew. Chem. Int. Ed.* **2008**, *47*, 4966–4981.

[3] a) D. G. Samsonenko, H. Kim, Y. Sun, G.-H. Kim, H.-S. Lee, K. Kim, *Chem. Asian J.* **2007**, *1*, 484–488; b) S. Ma, X.-S. Wang, C. D. Collier, E. S. Manis, H.-C. Zhou, *Inorg. Chem.* **2007**, *46*, 8499–8501.

[4] a) O. M. Yaghi, G. M. Li, H. L. Li, *Nature* **1995**, *378*, 703–706; b) H. Li, M. Eddaoudi, M. O'Keeffe, O. M. Yaghi, *Nature* **1999**, *402*, 276–279; c) N. L. Rosi, J. Eckert, M. Eddaoudi, D. T. Vodak, J. Kim, M. O'Keeffe, O. M. Yaghi, *Science* **2003**, *300*, 1127–1129.

[5] a) M. Kondo, T. Yoshitomi, K. Seki, H. Matsuzaka, S. Kitagawa, *Angew. Chem.* **1997**, *109*, 1844–1846; *Angew. Chem. Int. Ed. Engl.* **1997**, *36*, 1725–1727; b) M. Kondo, T. Okubo, A. Asami, S. Noro, T. Yoshitomi, S. Kitagawa, T. Ishii, H. Matsuzaka, K. Seki, *Angew. Chem.* **1999**, *111*, 190–193; *Angew. Chem. Int. Ed.* **1999**, *38*, 140–143.

[6] N. Rosi, M. Eddaoudi, D. Vodak, J. Eckert, M. O'Keeffe, O. M. Yaghi, *Science* **2003**, *300*, 1127–1129.

[7] F. X. Llabrés i Xamena, A. Abad, A. Corma, H. Garcia, *J. Catal.* **2007**, *250*, 294–298.

[8] a) T. Uemura, S. Horike, S. Kitagawa, *Chem. Asian J.* **2006**, *1–2*, 36–44; b) T. K. Maji, S. Kitagawa, *Pure Appl. Chem.* **2007**, *79*, 2155–2177; c) B. D. Chandler, G. D. Enright, K. A. Udachin, S. Pawsey, J. A. Ripmeester, D. T. Cramb, G. K. H. Shimizu, *Nat. Mater.* **2008**, *7*, 229–235; d) H. A. Habib, J. Sanchiz, C. Janiak, *Dalton Trans.* **2008**, 1734–1744.

[9] a) D. Maspoch, D. Ruiz-Molina, J. Veciana, *Chem. Soc. Rev.* **2007**, *36*, 770–818; b) A. Galet, M. C. Muñoz, J. A. Real, *Chem. Commun.* **2006**, 4321–4323 c) F. Gándara, A. de Andrés, B. Gómez-Lor, E. Gutiérrez-Puebla, M. Iglesias, M. A. Monge, D. M. Proserpio, N. Snejko, *Cryst. Growth Des.* **2008**, *8*, 378–382; d) B. V. Harbuzaru, A. Corma, F. Rey, P. Atienzar, J. L. Jordá, H. García, D. Ananias, L. D. Carlos, J. Rocha, *Angew. Chem.* **2008**, *120*, 1096–1099; *Angew. Chem. Int. Ed.* **2008**, *47*, 1080–1083.

[10] N. Masciocchi, S. Bruni, E. Cariati, F. Cariati, S. Galli, A. Sironi, *Inorg. Chem.* **2001**, *40*, 5897–5905.

[11] a) H. Hayashi, A. P. Côté, H. Furukawa, M. O'Keeffe, O. M. Yaghi, *Nat. Mater.* **2007**, *6*, 501–506; b) K. S. Park, Z. Ni, A. P. Côté, J. Y. Choi, R. Huang, F. J. Uribe-Romo, H. K. Chae, M. O'Keeffe, O. M. Yaghi, *Proc. Natl. Acad. Sci. USA* **2006**, *103*, 10186–10191; c) X.-C. Huang, Y.-Y. Lin, J.-P. Zhang, X.-M. Chen, *Angew. Chem.* **2006**, *118*, 1587–1589; *Angew. Chem. Int. Ed.* **2006**, *45*, 1557–1559; d) Y.-Q.

Tian, Y.-M. Zhao, Z.-X. Chen, G.-N. Zhang, L.-H. Weng, D.-Y. Zhao, *Chem. Eur. J.* **2007**, *13*, 4146–4154; e) R. Banerjee, A. Phan, B. Wang, C. Knobler, H. Furukawa, M. O'Keeffe, O. M. Yaghi, *Science* **2008**, *319*, 939–943.

[12] E. Barea, M. A. Romero, J. A. R. Navarro, J. M. Salas, N. Masciocchi, S. Galli, A. Sironi, *Inorg. Chem.* **2005**, *44*, 1472–1481.

[13] N. Masciocchi, S. Galli, A. Sironi, E. Cariati, M. A. Galindo, E. Barea, M. A. Romero, J. M. Salas, J. A. R. Navarro, F. Santoyo-González, *Inorg. Chem.* **2006**, *45*, 7612–7620.

[14] E. Barea, J. A. R. Navarro, J. M. Salas, N. Masciocchi, S. Galli, A. Sironi, *J. Am. Chem. Soc.* **2004**, *126*, 3014–3015, and references therein.

[15] J. A. R. Navarro, E. Barea, J. M. Salas, N. Masciocchi, S. Galli, A. Sironi, C. O. Ania, J. B. Parra, *J. Mater. Chem.* **2007**, *17*, 1939–1946.

[16] J. A. R. Navarro, E. Barea, J. M. Salas, C. O. Ania, J. B. Parra, N. Masciocchi, S. Galli, A. Sironi, *J. Am. Chem. Soc.* **2008**, *130*, 3978–3984.

[17] S. Ma, X.-S. Wang, D. Yuan, H.-C. Zhou, *Angew. Chem.* **2008**, *120*, 4198–4201; *Angew. Chem. Int. Ed.* **2008**, *47*, 4130–4133.

[18] G. W. Stinton, J. S. O. Evans, *Appl. Crystallogr.* **2007**, *40*, 87–95.

[19] J. A. R. Navarro, E. Barea, M. A. Galindo, J. M. Salas, M. A. Romero, M. Quirós, N. Masciocchi, S. Galli, A. Sironi, B. Lippert, *J. Solid State Chem.* **2005**, *178*, 2436–2451.

[20] G. A. Ardizzoia, G. La Monica, N. Masciocchi, A. Maspero, A. Sironi, *Eur. J. Inorg. Chem.* **2000**, 2507–2515.

[21] The percent empty volume has been estimated with PLATON (A. L. Spek, *J. Appl. Crystallogr.* **2003**, *36*, 7–13) with a probe sphere of 1.2 Å radius, after elimination of the guest water molecules, if any.

[22] E. Barea, J. A. R. Navarro, J. M. Salas, N. Masciocchi, S. Galli, A. Sironi, *Inorg. Chem.* **2004**, *43*, 473–481.

[23] N. Masciocchi, S. Galli, A. Sironi, E. Barea, J. A. R. Navarro, J. M. Salas, L. C. Tabares, *Chem. Mater.* **2003**, *15*, 2153–2160.

[24] P. A. Wright, *Microporous Framework Solids*, RSC, Cambridge, **2008**.

[25] F. Rouquerol, J. Rouquerol, K. Sing, *Adsorption by Powders and Porous Solids*, Academic Press, London **1999**.

[26] D. Tanaka, S. Kitagawa, *Chem. Mater.* **2008**, *20*, 922–931.

[27] P. L. Llewellyn, S. Bourrelly, C. Serre, Y. Filinchuk, G. Férey, *Angew. Chem.* **2006**, *118*, 7915–7918; *Angew. Chem. Int. Ed.* **2006**, *45*, 7751–7754.

[28] J. A. R. Navarro, E. Barea, J. M. Salas, N. Masciocchi, S. Galli, A. Sironi, C. O. Ania, J. B. Parra, *Inorg. Chem.* **2006**, *45*, 2397–2399.

[29] a) V. Sánchez, A. Storr, R. C. Thompson, *Can. J. Chem.* **2002**, *80*, 133–140; b) Y.-Q. Tian, C.-X. Cai, Y. Ji, X.-Z. You, *Angew. Chem.* **2002**, *114*, 1442–1444; *Angew. Chem. Int. Ed.* **2002**, *41*, 1384–1386.

[30] A. B. P. Lever, *Inorganic Electronic Spectroscopy*, Elsevier, Amsterdam, **1984**.

[31] Y. Dou, *J. Chem. Educ.* **1990**, *67*, 134.

[32] a) M. E. Lines, *J. Phys. Chem. Solids* **1970**, *31*, 101–116; b) G. S. Rushbrooke, P. J. Wood, *Mol. Phys.* **1958**, *1*, 257–283.

[33] J. A. R. Navarro, E. Barea, J. M. Salas, N. Masciocchi, S. Galli, A. Sironi, *Inorg. Chem.* **2007**, *46*, 2988–2997.

[34] For a recent example see H. Casellas, O. Roubeau, S. J. Teat, N. Masciocchi, S. Galli, A. Sironi, P. Gamez, J. Reedijk, *Inorg. Chem.* **2007**, *46*, 4583–4591.

[35] A. A. Coelho, *J. Appl. Crystallogr.* **2003**, *36*, 86–95.

[36] Topas-R: General profile and structure analysis software for powder diffraction data; Bruker AXS, Karlsruhe (Germany), **2001**.

[37] H. Toraya, *J. Appl. Crystallogr.* **1986**, *19*, 440–447.

[38] A. A. Coelho, *J. Appl. Crystallogr.*. **2000**, *33*, 899–908.

[39] a) The geometry of the 5-F-2-pymo anion has been optimised at the B3LYP/6–311G(2d, 1p) level of theory using Gaussian 03W; b) Gaussian 03 (Revision C.02), M. J. Frisch, G. W. Trucks, H. B. Schlegel, G. E. Scuseria, M. A. Robb, J. R. Cheeseman, J. A. Montgomery Jr., T. Vreven, K. N. Kudin, J. C. Burant, J. M. Millam, S. S. Iyengar, J. Tomasi, V. Barone, B. Mennucci, M. Cossi, G. Scalmani, N. Rega, G. A. Petersson, H. Nakatsuji, M. Hada, M. Ehara, K. Toyota, R. Fukuda, J. Hasegawa, M. Ishida, T. Nakajima, Y. Honda, O. Kitao, H. Nakai, M. Klene, X. Li, J. E. Knox, H. P. Hratchian, J. B. Cross, C. Adamo, J. Jaramillo, R. Gomperts, R. E. Stratmann, O. Yazyev, A. J. Austin, R. Cammi, C. Pomelli, J. W. Ochterski, P. Y. Ayala, K. Morokuma, G. A. Voth, P. Salvador, J. J. Dannenberg, V. G. Zakrzewski, S. Dapprich, A. D. Daniels, M. C. Strain, O. Farkas, D. K. Malick, A. D. Rabuck, K. Raghavachari, J. B. Foresman, J. V. Ortiz, Q. Cui, A. G. Baboul, S. Clifford, J. Cioslowski, B. B. Stefanov, G. Liu, A. Liashenko, P. Piskorz, I. Komaromi, R. L. Martin, D. J. Fox, T. Keith, M. A. Al-Laham, C. Y. Peng, A. Nanayakkara, M. Challacombe, P. M. W. Gill, B. Johnson, W. Chen, M. W. Wong, C. Gonzalez, J. A. Pople, Gaussian, Inc., Pittsburgh, PA, **2004**.

[40] R. W. Cheary, A. Coelho, *J. Appl. Crystallogr.* **1992**, *25*, 109–121.

[41] a) A. March, *Z. Kristallogr. Kristallgeom. Kristallphys. Kristallchem.* **1932**, *81*, 285–297; b) W. A. Dollase, *J. Appl. Crystallogr.* **1986**, *19*, 267–272.

Received: May 30, 2008
Published online: October 8, 2008

